Optical Phase Properties of Small Numbers of Nanoslits and an Application for Higher-efficiency Fresnel Zone Plates

Hyuntai Kim[1] and Seung-Yeol Lee[2]*

[1]Department of Electronic & Electrical Convergence Engineering, Hongik University, Sejong 30016, Korea
[2]School of Electronics Engineering, Kyungpook National University, Daegu 41566, Korea

We have studied the behavior of light in the intermediate regime between a single nanoslit and an infinite nanoslit array. We first calculated the optical characteristics of a small number of nanoslits using finite element numerical analysis. The phase variance of the proposed nanoslit model shows a gradual phase shift between a single nanoslit and ideal nanoslit array, which stabilizes before the total array length becomes ~0.5 λ. Next, we designed a transmission-enhanced Fresnel zone plate by applying the phase characteristics from the small-number nanoslit model. The virtual-point-source method suggests that the proposed Fresnel zone plate with phase-invariant nanoslits achieves 2.34x higher transmission efficiency than a conventional Fresnel zone plate. Our report describes the intermediate behaviors of a nanoslit array, which could also benefit subwavelength metallic structure research of metasurfaces.

Keywords : Metamaterial, Effective medium theory, Nanoslit array, Fresnel zone plate
OCIS codes : (240.6680) Surface plasmons; (050.1380) Binary optics; (220.3630) Lenses

I. INTRODUCTION

Since the development of nano-fabrication technology, researchers have extensively studied nanophotonics [1-3]. Structures that are smaller than the optical wavelength will effectively respond as a homogeneous layer and are called metamaterials or metasurfaces [4-7]. Metasurfaces, which consist of sub-wavelength artificially-designed meta-atoms, can control the wavefront of the transmitted or reflected incident light due to the optical response of the meta-atoms within a thin layer. Researchers have studied numerous metasurfaces for various applications such as shaping waves, focusing, angular momentum generation, and high harmonic generation [8-12].

Binary structures such as nano-holes and nanoslits have received a great deal of interest. These surfaces have several advantages, including fascinating phase-based focusing characteristics, ease of fabrication, and flexibility when applied to other thin film binary structures such as Fresnel zone plates. Recently, researchers have applied binary structures to develop ultra-compact devices for polarizing, plasmonic switching, and super-resolution focusing [13-17].

Although many publications describe dedicated theoretical, numerical, and experimental studies to understand meta-atoms and arrays of meta-atoms, we found few studies that analyze the characteristics of a small number of meta-atoms, which is more complex than a single meta-atom or its ideal array. As the demand for metasurface increases, researchers require a deeper understanding of how the optical characteristics depend on the number of meta-atoms. For example, some applications use a group of meta-atoms as a super-pixel [18], so each pixel region is composed of a few meta-atoms that show different characteristics than an infinite number of meta-atoms.

We therefore chose to study the intermediate zone, defined as a small number of nanoslits that does not match the optical characteristics of either a nanoslit or a nanoslit array. Using numerical simulations based on the finite element method, we have analyzed the transmission characteristics of the intermediate zone; we also mapped

*Corresponding author: seungyeol@knu.ac.kr, ORCID 0000-0002-8987-9749

Color versions of one or more of the figures in this paper are available online.

the phase evolution between a single, a few, and an infinite number of nanoslits. Based on these results and the virtual point method [19], we designed a novel transmission-enhanced (TE) metallic Fresnel zone plate (MFZP) which improves the focusing efficiency by 2.34x compared to a standard FZP. We believe that our studies on intermediate numbers of meta-atoms will be a key tool when designing metasurfaces with nonuniform distributions, especially when the metasurfaces include narrow regions that only allow a limited number of meta-atoms.

II. OPTICAL CHARACTERISTICS OF A FEW NANOSLITS

Researchers have studied single metallic slits and infinite slit arrays in various manners. For example, the waveguide solution of a single slit requires Maxwell's equations to solve for the boundary conditions at the edge of the slit, assuming infinite thickness. On the other hand, effective medium theory (EMT) and the cavity mode approach work well to explain the characteristics of infinite slit arrays. The EMT regards the slit array aligned in the x direction as a single material relative to each polarization, as shown in the equation

$$n_{eff,x} = \frac{1}{\sqrt{\dfrac{f}{n_1} + \dfrac{1-f}{n_2}}}, \; n_{eff,y} = \sqrt{fn_1 + (1-f)n_2} \quad (1)$$

where $n_{eff,x}$ and $n_{eff,y}$ are the effective refractive index for x polarized and y polarized incident waves, respectively, n_1 and n_2 are the refractive indices of each material, and f is the duty factor [20].

However, both the analytic solution and the EMT approach have limitations. The analytic solution based on a cavity mode assumes that the thickness of the metal is relatively thick compared to the wavelength and that the slit width is extremely narrow. On the other hand, the EMT approach is only valid for infinite arrays of slits and for situations where the wave is equally distributed inside the metallic and gap regions, resulting in significant errors for slits that are thick or wide compared to the incident wavelength.

Neither the analytic solution nor the EMT approach is applicable for a small number of nanoslits. As the demand for metasurfaces increases, we need to better understand the intermediate zone behavior between single and infinite arrays of the unit meta-atom before we can successfully apply metasurfaces to irregular surfaces. Therefore, we analyze the intermediate zone in this paper - which we define as a system consisting of a small number of nanoslits as shown in Fig. 1(a) - to create a more complete understanding of nanoslit-based structures.

We used numerical simulations to study the intermediate zone. We utilized a commercial program, COMSOL Multiphysics, for the full finite-element method (FEM) calculation and chose a free-space wavelength of 1064 nm for the incident beam, a typical value for Ytterbium-doped lasers [21]. We gradually increased the number of nanoslits and calculated the accumulated phase evolution of the structure.

In the 2D slit design, we can control four parameters - the number of slits (n), the slit width (s), the duty cycle (f), and the metal thickness (t). To isolate the effects of each parameter as we analyze the intermediate zone behavior, we varied the slit number and one of the other geometric properties while freezing the other two values. Figure 1 shows the schematic and the simulation conditions. Note that we increased the thickness of the slit-free metallic region by 0.5 μm between the end of the slit array and the 1μm perfectly matched layer (PML) to ensure an accurate transmission calculation.
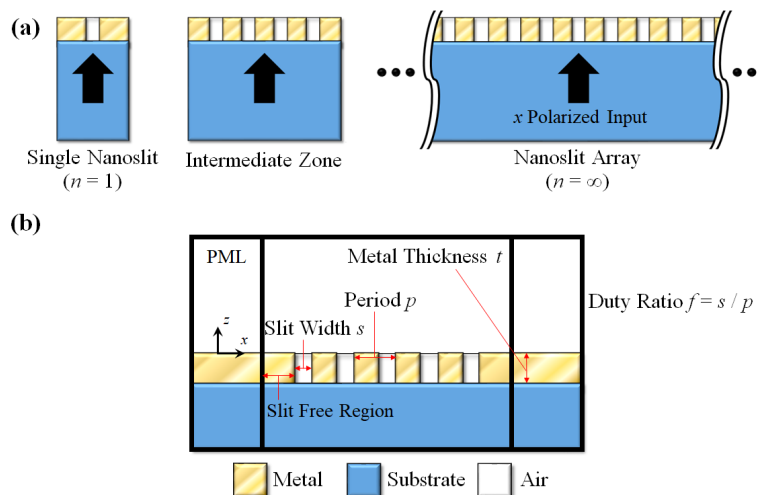

FIG. 1. (a) Schematic of a single nanoslit, the intermediate zone, and an infinite nanoslit array. (b) Parameter descriptions and simulation conditions of the nanoslit array.

In general, the transmitted amplitude and the phase determine the properties of the typical non-diffractive subwavelength geometry [22-26]. We focused on the phase change characteristics rather than the amplitude change because we have found that the field distribution of the transmitted light, whether focused or diffracted, is mainly determined by the spatial phase shift of each element. This study confirmed our position since the transmitted amplitude shows typical changes in amplitude characteristics that are proportional to the total length of the slit arrays and the opening portion.

First, we varied the duty cycle with a fixed slit width of $s = 90$ nm and a fixed thickness of $t = 300$ nm. Figure 2(a) shows the phase differences at the slit array. For a single slit, the duty cycle does not change the structure, so all of the curves start at an identical value. As the number of nanoslits increases, the transmission phase curves start to fluctuate between two and six slits, but eventually the
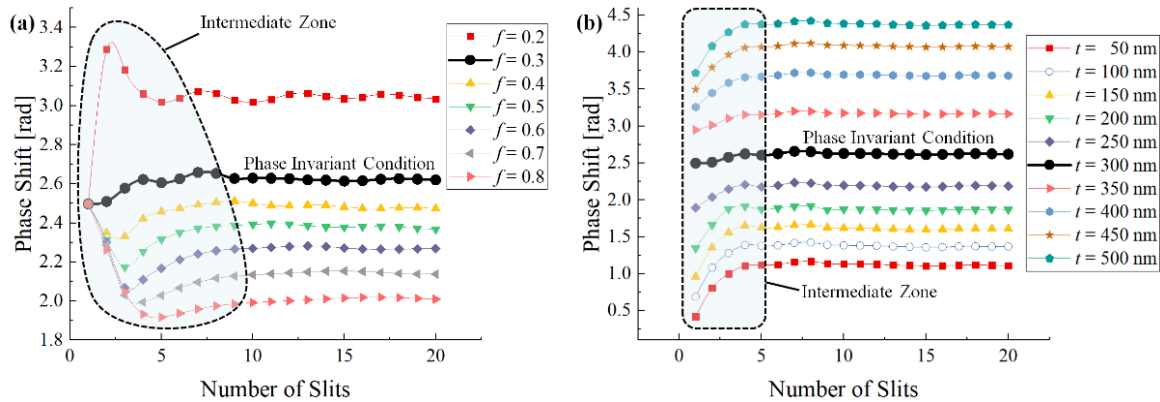

FIG. 2. Optical phase shift vs. number of slits when (a) varying duty cycle and (b) varying thickness. The phase-invariant conditions are marked by thick black lines.
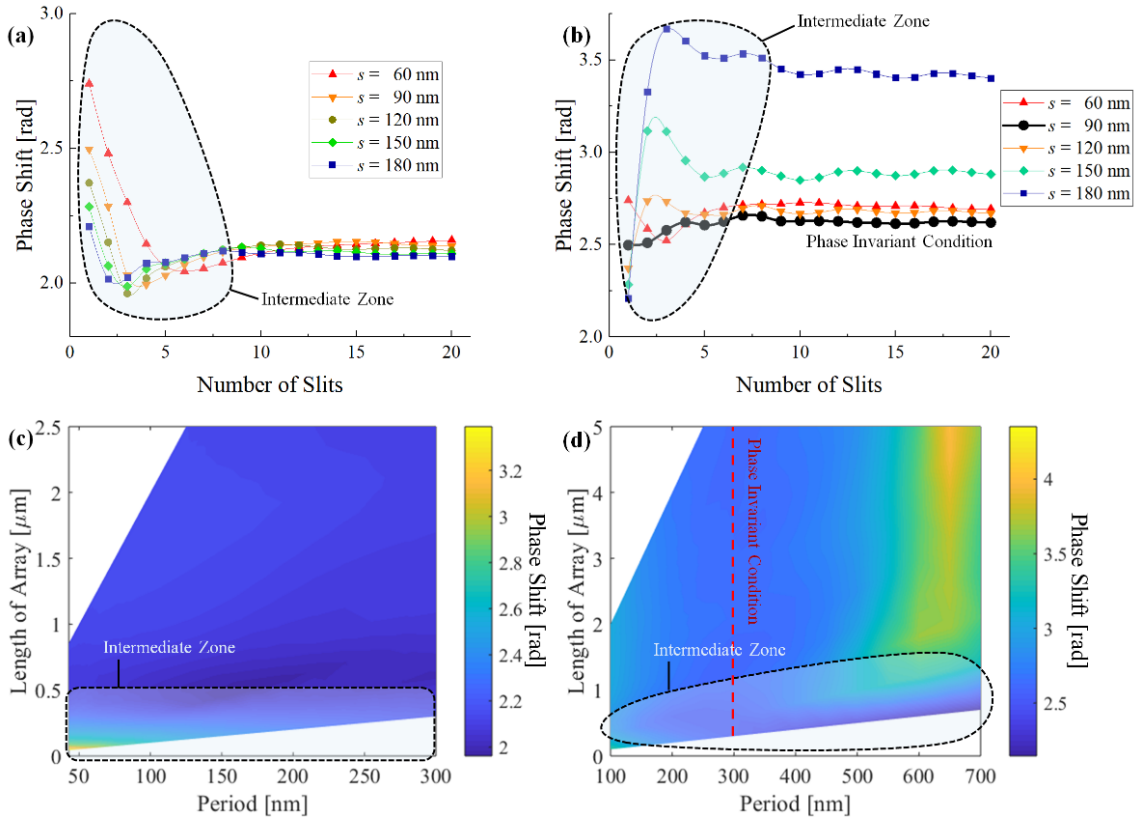

FIG. 3. Phase shift vs. number of slits for various slit widths at duty cycles of (a) 0.7 and (b) 0.3. Phase shift vs. period and total array length at duty cycles of (c) 0.7 and (d) 0.3. The phase-invariant conditions are marked by a thick black line in Fig. 3(b) and a dashed red line in Fig. 3(d).

curves approach a specific value; the intermediate region between two and six slits is marked by a dashed closed loop. We note the specific condition of an $f = 0.3$ duty cycle as a phase-invariant condition where the transmission phase fluctuation is minimized. We will use this condition in the next section to design a TE-MFZP. The EMT predicts that a higher duty cycle will cause a lower phase shift, which agrees with our numerical results: the saturated phase difference gradually decreases as the value of f increases.

Likewise, we expect an increase in the metal thickness to linearly increase the transmission phase shift for both the waveguide and EMT models, assuming that the multiple reflections at the end of aperture are small enough. To confirm this hypothesis, we performed numerical simulations where we varied the metal thickness layer under the condition of $s = 90$ nm and $f = 0.3$. Figure 2(b) shows parallel curve shifts as we predicted. By optimizing to $t = 300$ nm, we once again significantly reduce the phase shift fluctuation within the intermediate zone.

Figure 3 shows the optical phase shift response when we vary the slit width for a fixed duty cycle and thickness. If we only consider the theoretical EMT calculation, the phase shift of a slit array with a fixed duty cycle and thickness would be constant since Eq. (1) is only a function of the material refractive indices and duty cycle. Since the metallic region is highly lossy, however, the field cannot fully interact with the metal structure when the metal is too thick or too wide [22].

When we compare the transmitted phase profile with a metal thickness of 300 nm and a duty cycle of 0.7 and 0.3, as shown in Figs. 3(a) and 3(b), we note that a sufficiently high duty cycle ($f = 0.7$) causes all of the values to converge to a similar value regardless of the slit width. This result means the EMT theory matches the true performance well when the metallic portion is narrow. The EMT theory also holds when the duty cycle is 0.3 for thin slit width cases ($s < 140$ nm), as seen by these cases converging to a similar value. The EMT assumption breaks as the metallic region width increases, however, and the phase shift approaches different values depending on the value of s and n.

Figures 3(c) and 3(d) are reconstructed from Figs. 3(a) and 3(b) with an x-axis of period (s / f) instead of slit width (s) and a y-axis showing the total array length ($n \, s / f$) instead of the number of slits (n). We note that, before the total length reaches 0.5 λ, the transmitted phase approaches the final value. For array lengths over 0.5 λ, each slit component exceeds the size of the meta-atom and acts as an individual point source. This result shows that the total length determines the phase stabilization point, rather than the number of slits; the phase transmitted by a small cluster of meta-atoms is equivalent to the phase from an infinite number of meta-atoms when the small cluster is larger than about a half wavelength.

III. DESIGN OF A TRANSMISSION-ENHANCED MFZP

MFZPs have been used for several focusing and metasurface applications because they are thin and require simple structures. Given that these optics block almost half of the transmitted light, however, researchers have found few practical uses that can tolerate this low transmission efficiency.

We were inspired by the two facts that 1) a subwavelength periodic nanoslit array has a different transmitted phase than the fully-open air region and 2) we can design this transmitted phase to be invariant to the number of slits by optimizing slit geometries. We therefore believed that we could increase the transmission efficiency MFZPs by replacing a portion of the blocked region with nanoslit arrays.

Since the open portions of the MFPZ have different widths, we need to use different amounts of nanoslits in each region; the transmitted phase of each nanoslit must be invariant regardless of the number of slits. Section 2 showed that the transmitted phase of the intermediate zone gradually approaches the phase of an infinite slit array for every slit geometry that we have simulated. We expect that, if the transmitted phase of a single slit is similar to the phase of an infinite slit array, the phase response of the intermediate zone would also be relatively constant. These phase-invariant conditions are highlighted in Figs. 2 and 3 with a thick black line and circle markers and dashed red lines, respectively. Under the condition of $f = 0.3$, $s = 90$ nm, and $t = 300$ nm, we achieved a 0.04 rad standard deviation from a single slit to twenty slits. We would like to point out that this phase-invariant condition with respect to the number of slits could be useful on other phase-based applications, not only for MFZPs.

We designed the TE-MFZP using virtual point source design [19], which produces the following equation for an MFZP mask.

$$M[\phi,x,f_0] = sign\left[real\left\{\exp\left(k\left(x^2 + f_0^2\right)^{1/2} + \phi\right)\right\}\right] \tag{2}$$

where f_0 is the lens focal length, ϕ is the phase of the virtual point source, and x is the mask position. The output of the "sign" function is 1 when the input is positive and 0 when the input is zero or negative. Figure 4 shows the two different MFZP masks with a source phase difference of $\Delta\phi$ in blue ($M[\phi_0]$) and red ($M[\phi_0 + \Delta\phi]$). If every other parameter - such as metal thickness and source conditions - is identical, the virtual point source generated by these two masks will have a phase difference of $\Delta\phi$.

We use this approach to substitute the open region with nanoslit arrays and shift the phase of the focused light by the phase difference between free space and the nanoslit. When we set $\Delta\phi$ to the average phase shift of the phase-invariant condition, the focused light from the blue
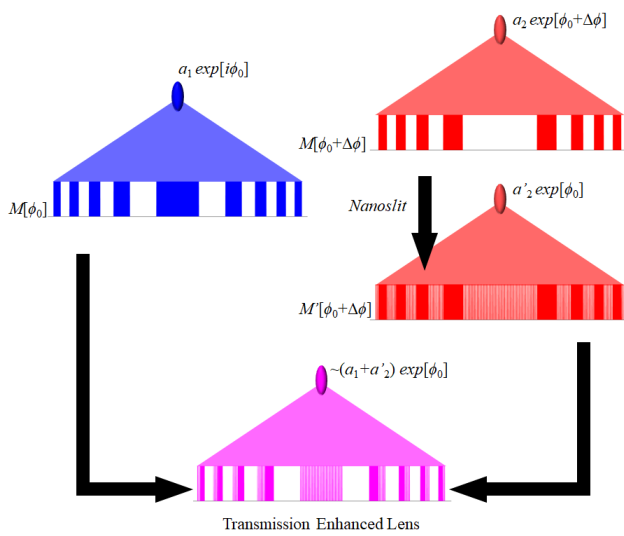
FIG. 4. Plate design mechanism of the TE-MFZP based on virtual point source.

that would previously have been blocked. Since we need to obtain a constant phase shift from both the wide and narrow regions of the slit-assisted region, our use of phase-invariance is quite important. We chose the average value because, even for the phase-invariant condition, there are slight fluctuations between different numbers of slits.

This proposed TE-MFZP allows a brighter focus for the x-polarized component thanks to the additional transmitted light from the nanoslit array, which shows an almost-uniform phase profile for different numbers of slits. Although the schematic we include is for a 1D line-beam-focusing MFZP, our result is also applicable to 2D MFZPs.

For the TE-MFZP shown in Fig. 5, we chose a target focal length of $f_0 = 40$ μm and we optimized the initial phase to maximize the area to be filled by nanoslit arrays. For the nanoslit array regime, we choose the phase-invariant condition that we described previously: $f = 0.3$, $s = 90$ nm, and $t = 300$ nm. Using these conditions, we determined that the average phase shift was 2.61 ± 0.04 rad, which has $\Delta\phi = 0.84$ rad difference relative to the 300 nm phase propagation in free space. The field patterns of the conventional MFZP and TE-MFZP, when illuminated by x-polarized light, are shown in Figs. 5(a) and 5(b), respectively. These patterns clearly show that the TE-MFZP collects more light from the incidence wave; the energy at

plate $M[\phi_0]$ and the nanoslit-assisted plate $M'[\phi_0 + \Delta\phi]$ will generate foci with identical locations and phase. Therefore, if we combine two plates as shown in Fig. 4, the new hybridized MFZP will focus light from the nanoslit region
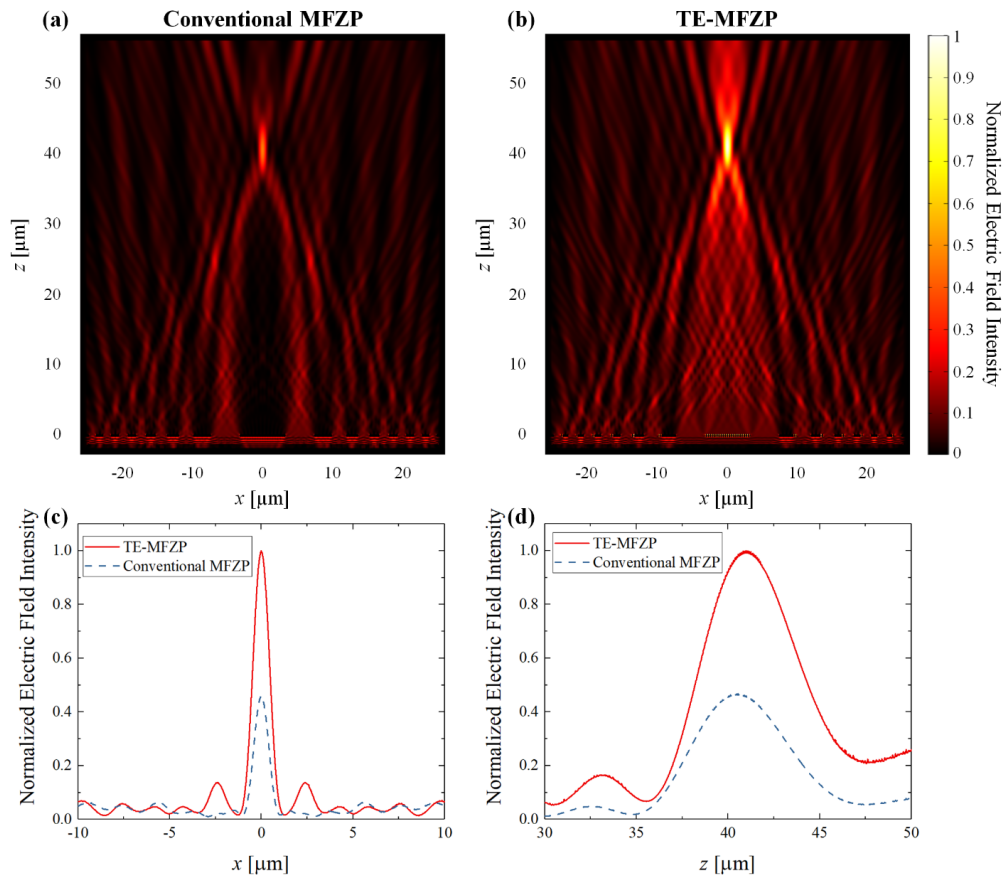

FIG. 5. Field intensity of (a) the conventional MFZP and (b) the TE-MFZP. Cross-sections of the field intensity (c) perpendicular and (d) parallel to the propagation axis for an x-polarized input beam.

the focus has increased from 9.6% to 22.5% of the incident energy, a 2.34x improvement. We calculate the focal efficiency as the ratio of the power flux at the focused point to the input beam and we measure the power of the focused beam by integrating the Poynting vector.

Figures 5(c) and 5(d) show cross-sections of the electric field intensity, normalized to the peak intensity of the TE-MFZP. Figure 5(c) depicts the field at the focal plane ($z = 40$ μm) and Fig. 5(d) depicts the field along the propagation axis at $x = 0$. These cross-sections show that the peak intensity at the focus has increased by a factor of 2.14. Although the focal length has slightly shifted, the increase from 40 μm to 40.99 μm is less than 2.5%, which we consider an acceptable modification given the increase in peak field intensity at the focal plane.

Although we only show the one-dimensional MFZP simulation results, we expect that our proposed concept based on phase-invariant nanoslit arrays is also valid for circularly-shaped 2D FZPs. We also believe that, by changing the fill layers of the secondary FZP from nanoslits to nano-holes or nano-apertures, this scheme will improve the efficiency without a polarization dependency.

IV. CONCLUSION

To conclude, we have analyzed the intermediate regime between a single metallic slit and an infinite slit array and shown that the optical phase characteristics converged before the total array length reaches ~0.5 λ. In addition, we have discovered a regime where the phase property of the intermediate zone is relatively flat, which improves the efficiency of the MFZP. By starting with the virtual point source method, we designed a TE-MFZP and achieved 2.34x higher efficiency than a conventional MFZP. We believe that our study will increase interest in small clusters of meta-atoms and will be useful when designing binary metallic structures.

ACKNOWLEDGMENT

REFERENCES

1. M. L. Brongersma and P. G. Kik, *Surface plasmon nano-photonics* (Springer, Dordrecht, 2007).
2. H. Lan and Y. Ding, "Nanoimprint lithography," in *Lithography*, M. Wang. ed. (InTechOpen, London, UK, 2010), pp. 457-494.
3. H. Kim, "Plasmonics on optical fiber platforms," in *Plasmonics*, T. Gric. ed. (IntechOpen, London, UK, 2018), Chapter 10.
4. F. Qin, L. Ding, L. Zhang, F. Monticone, C. C. Chum, J. Deng, S. Mei, Y. Li, J. Teng, M. Hong, S. Zhang, A. Alù, and C.-W. Qiu, "Hybrid bilayer plasmonic metasurface efficiently manipulates visible light," Sci. Adv. **2**, e1501168 (2016).
5. D. Lin, P. Fan, E. Hasman, and M. L. Brongersma, "Dielectric gradient metasurface optical elements," Science **345**, 298-302 (2014).
6. D. Schurig, J. J. Mock, B. J. Justice, S. A. Cummer, J. B. Pendry, A. F. Starr, and D. R. Smith, "Metamaterial electromagnetic cloak at microwave frequencies," Science **314**, 977-980 (2006).
7. N. Engheta and R. W. Ziolkowski, *Metamaterials: Physics and engineering explorations* (John Wiley & Sons, US, 2006).
8. P. R. West, J. L. Stewart, A. V. Kildishev, V. M. Shalaev, V. V. Shkunov, F. Strohkendl, Y. A. Zakharenkov, R. K. Dodds, and R. Byren, "All-dielectric subwavelength metasurface focusing lens," Opt. Express **22**, 26212-26221 (2014).
9. S. Liu, M. B. Sinclair, S. Saravi, G. A. Keeler, Y. Yang, J. Reno, G. M. Peake, F. Setzpfandt, I. Staude, T. Pertsch, and I. Brener, "Resonantly enhanced second-harmonic generation using III-V semiconductor all-dielectric metasurfaces," Nano Lett. **16**, 5426-5432 (2016).
10. E. Karimi, S. A. Schulz, I. D. Leon, H. Qassim, J. Upham, and R. W. Boyd, "Generating optical orbital angular momentum at visible wavelengths using a plasmonic metasurface," Light: Sci. Appl. **3**, e167 (2014).
11. X. Yi, P. Huang, X. Huang, Z. Xu, C. Zhang, J. Zhao, X. Liu, Y. Ai, and H. Chen, "Operation of polarization order of vector beams with cascaded metasurfaces," Appl. Phys. B **123**, 243 (2017).
12. N. Nookala, J. Xu, O. Wolf, S. March, R. Sarma, S. Bank, J. Klem, I. Brener, and M. Belkin, "Mid-infrared second-harmonic generation in ultra-thin plasmonic metasurfaces without a full-metal backplane," Appl. Phys. B **124**, 132 (2018).
13. X. Ni, S. Ishii, A. V. Kildishev, and V. M. Shalaev, "Ultra-thin, planar, Babinet-inverted plasmonic metalenses," Light: Sci. Appl. **2**, e72 (2013).
14. S.-Y. Lee, K. Kim, G.-Y. Lee, and B. Lee, "Polarization-multiplexed plasmonic phase generation with distributed nanoslits," Opt. Express **23**, 15598-15607 (2015).
15. H. Kim, J. Kim, H. An, Y. Lee, G.-y. Lee, J. Na, K. Park, S. Lee, S.-Y. Lee, B. Lee, and Y. Jeong, "Metallic Fresnel zone plate implemented on an optical fiber facet for super-variable focusing of light," Opt. Express **25**, 30290-30303 (2017).
16. M. Khorasaninejad, W. T. Chen, R. C. Devlin, J. Oh, A. Y. Zhu, and F. Capasso, "Metalenses at visible wavelengths: Diffraction-limited focusing and subwavelength resolution imaging," Science **352**, 1190-1194 (2016).
17. E. T. Rogers, J. Lindberg, T. Roy, S. Savo, J. E. Chad, M. R. Dennis, and N. I. Zheludev, "A super-oscillatory lens optical microscope for subwavelength imaging," Nat. Mater. **11**, 432-435 (2012).
18. C. Choi, S.-J. Kim, J.-G. Yun, J. Sung, S.-Y. Lee, and B. Lee, "Deflection angle switching with a metasurface based

on phase-change nanorods," Chin. Opt. Lett. **16**, 050009 (2018).

19. J. Kim, H. Kim, G.-Y. Lee, J. Kim, B. Lee, and Y. Jeong, "Numerical and experimental study on multi-focal metallic Fresnel zone plates designed by the phase selection rule via virtual point sources," Appl. Sci. **8**, 449 (2018).

20. C. W. Haggans, L. Li, and R. K. Kostuk, "Effective-medium theory of zeroth-order lamellar gratings in conical mountings," J. Opt. Soc. Am. A **10**, 2217-2225 (1993).

21. Y. Jeong, L. A. Vazquez-Zuniga, S. J. Lee, G. Choi, Y. Kwon, and H. Kim, "High-power fiber lasers," in *Proc. 2012 17th Opto-Electronics and Communications Conference*, (Korea, Jul. 2012), pp. 580-581.

22. H. Kim and Y. Jeong, "Theoretical and numerical study of cylindrical-vector-mode radiation characteristics in periodic metallic annular slits and their applications," Curr. Opt. Photon. **2**, 482-487 (2018).

23. J. Kim, J. Kim, J. Na, and Y. Jeong, "Numerical study of a novel bi-focal metallic fresnel zone plate having shallow depth-of-field characteristics," Curr. Opt. Photon. **2**, 147-152 (2018).

24. H. Kim, "Metallic triangular pillar grating arrays for high transmission polarizers for air:glass interfaces," Jpn. J. Appl. Phys. **58**, 042001 (2019).

25. N. T. Trung, D. Lee, H. K. Sung, and S. Lim, "Angle-and polarization-insensitive metamaterial absorber based on vertical and horizontal symmetric slotted sectors," Appl Opt. **55**, 8301-8307 (2016).

26. S.-Y. Lee, "Design of a plasmonic switch using ultrathin chalcogenide phase-change material," Curr. Opt. Photon. **1**, 239-246 (2017).